

Inhibition of O-GlcNAc transferase renders prostate cancer cells dependent on CDK9

Harri M. Itkonen^{1,2,3*}, Ninu Poulouse^{4,5}, Rebecca E. Steele^{4,6}, Sara E. S. Martin^{2,7}, Zebulon G. Levine², Damien Y. Duveau⁸, Ryan Carelli³, Reema Singh^{4,5}, Alfonso Urbanucci^{1,9,10}, Massimo Loda^{3,11,12}, Craig J Thomas^{8,13}, Ian G. Mills^{1,4,5,*}, Suzanne Walker^{2,*}

Affiliations:

- ¹ Centre for Molecular Medicine Norway, Nordic European Molecular Biology Laboratory Partnership, Forskningsparken, University of Oslo, Oslo, 0349, Norway.
- ² Department of Microbiology, Blavatnik Institute, Harvard Medical School, Boston, MA, 02115, USA.
- ³ Department of Pathology and Laboratory Medicine, Weill Cornell Medicine, New York-Presbyterian Hospital, New York, NY, 10065, USA.
- ⁴ PCUK/Movember Centre of Excellence for Prostate Cancer Research, Centre for Cancer Research and Cell Biology (CCRCB), Queen's University Belfast, BT7 1NN, UK.
- ⁵ Nuffield Department of Surgical Sciences, University of Oxford, John Radcliffe Hospital, Oxford, OX3 9DU, UK.
- ⁶ Current address: Breast Cancer Now Toby Robins Research Centre, The Institute of Cancer Research, London, United Kingdom, SW3 6JB
- ⁷ Current address: Chemistry Department, The College of Wooster, 943 College Mall, Wooster, OH 44691, USA.
- ⁸ Division of Preclinical Innovation, National Center for Advancing Translational Sciences, National Institutes of Health, Rockville, MD 20850, USA.
- ⁹ Department of Core Facilities, Institute for Cancer Research, Oslo University Hospital, Oslo, 0379, Norway.
- ¹⁰ Department of Tumor Biology, Institute for Cancer Research, Oslo University Hospital, Oslo, 0379, Norway.
- ¹¹ The Broad Institute of Harvard and MIT, Cambridge, MA, USA.
- ¹² The New York Genome Center, New York, NY, USA.
- ¹³ Lymphoid Malignancies Branch, Center for Cancer Research, National Cancer Institute, National Institutes of Health, Bethesda, MD 20892, USA.

Running title

Combinatorial lethality of OGT and CDK9 inhibitors

Corresponding authors:

1. Harri M Itkonen (Belfer Research Building, 413 E 69th St, New York, NY 10021; 212 746 6464; h.m.itkonen@gmail.com)
2. Ian G. Mills (Nuffield Department of Surgical Sciences, John Radcliffe Hospital, Headington, Oxford, OX3 9DU; ian.mills@linacre.ox.ac.uk)
3. Suzanne Walker (Harvard Medical School, 4 Blackfan Circle Boston, MA 02115; 617 432-5498; suzanne_walker@hms.harvard.edu)

Conflicts of Interest: The authors declare no potential conflicts of interest

Word count (excluding title page, abstract, references and figure legends): 3727

Total number of figures: 6 main figures

Tables: 0

Abstract

O-GlcNAc transferase (OGT) is a nutrient-sensitive glycosyltransferase that is overexpressed in prostate cancer, the most common cancer in males. We recently developed specific and potent inhibitor targeting this enzyme, and here we report a synthetic lethality screen using this compound. Our screen identified pan-cyclin-dependent kinase (CDK) inhibitor AT7519 as lethal in combination with OGT inhibition. Follow-up chemical and genetic approaches identified CDK9 as the major target for synthetic lethality with OGT inhibition in prostate cancer cells. OGT expression is regulated through retention of the fourth intron in the gene and CDK9 inhibition blunted this regulatory mechanism. CDK9 phosphorylates carboxy-terminal domain (CTD) of RNA Polymerase II (RNA Pol II) to promote transcription elongation. We show that OGT inhibition augments effects of CDK9 inhibitors on CTD phosphorylation and general transcription. Finally, the combined inhibition of both OGT and CDK9 blocked growth of organoids derived from metastatic prostate cancer patients but had minimal effects on normal prostate spheroids. We report a novel synthetic lethal interaction between inhibitors of OGT and CDK9 that specifically kills prostate cancer cells but not normal cells. Our study highlights the potential of combining OGT inhibitors with other treatments to exploit cancer specific vulnerabilities.

Implications: The primary contribution of OGT to cell proliferation is unknown, and in this study we use a compound screen to indicate that OGT and CDK9 collaborate to sustain a cancer cell specific pro-proliferative program. A better understanding of how OGT and CDK9 cross-talk will refine our understanding of this novel synthetic lethal interaction.

Introduction

O-GlcNAc transferase (OGT) is a nutrient-sensitive glycosyltransferase that modifies serine and threonine residues of nuclear and cytoplasmic proteins via single sugar conjugation to regulate their functions (1-3). Analogous to phosphorylation, this sugar mark can be removed by an enzyme termed O-GlcNAcase (OGA). However, unlike phosphorylation, which is regulated by hundreds of kinases, OGT is solely responsible for all nucleocytoplasmic glycosylation. As such, this enzyme is a unique sensor and regulator of cell function.

OGT and OGT's catalytic product, O-GlcNAcylation, are increased in many cancers, including prostate cancer, which is the most common cancer in males in the United States (4). Both OGT and O-GlcNAc levels correlate with aggressive disease (5,6), and OGT knockout results in a complete loss of proliferation (7-9). Development of specific OGT inhibitors is essential for probing the functions of this unique enzyme.

We recently developed a family of OGT small molecule inhibitors (OSMI-2 and OSMI-4) that bind in the OGT's active site with nanomolar dissociation constants (10). OSMI-2 and OSMI-4 reduce O-GlcNAc levels in multiple cell lines, but cells also rapidly respond by increasing OGT expression to compensate. Cells that are able to compensate for inhibition have limited overall transcriptomic and proteomic changes, providing evidence that these inhibitors have minimal off-target effects (10,11). There are modest growth-suppressive effects on cells; however, we wondered if the adaptations needed to respond to OGT inhibition may sensitize cancer cells to disruption of other cellular pathways.

In the current study, we screened 5000 bioactive compounds for synergism with OSMI-2 and identified the compound AT7519 as synthetically lethal with OGT inhibition in prostate cancer cells. AT7519 is a pan-cyclin-dependent kinase (CDK) inhibitor and here we show that reducing CDK9 activity is sufficient for synthetic lethality. The OGT inhibitor potentiated the effect of several structurally-unrelated, clinically relevant CDK9 inhibitors on RNA Pol II CTD phosphorylation, transcription and anti-proliferative effects on prostate cancer organoids. To conclude, prostate cancer cells become dependent on high OGT activity when CDK9 is inhibited, and our study proposes that OGT can be targeted to sensitize cancer cells to other treatments.

Materials and Methods

Cell culture and statistical analysis

LNCaP, C4-2, 22RV1, PC3, HCT116, MDAMB231 and RWPE-1 cells were obtained from ATCC, PNT2 cells were obtained from Sigma and all cell lines were maintained as recommended by the provider. Cells were authenticated using short tandem repeat profiling performed by ATCC.

Mycoplasma testing was performed regularly, using the colorimetric MycoAlert mycoplasma detection kit (Lonza). LNCaP-95 cells and MSK-PCA3 (12) model were kindly provided by Dr. M. Brown (Dana-Farber Cancer Institute, DFCI) and Dr. Yu Chen (Memorial Sloan Kettering Cancer Center), respectively. LNCaP-95 cells were maintained in 10% charcoal-stripped serum in phenol red-free RPMI. MSK-PCA3 cells were maintained as previously reported (13). Organoid experiments were performed in 12-well plates and all the experiments represent at least two biological replicates. Organoids were allowed to form in Matrigel domes for 3-10 days prior to treatment. After this, media was changed every 4-7 days, coinciding with imaging using a Zeiss AxioObserver inverted widefield microscope (Plan-Apochromat 20x/0.8). The growth of the cells in Matrigel was measured manually and is presented as change in the organoid size relative to the start of the treatments. For all statistical analysis presented in the manuscript, p-values are from two-sided analysis unless otherwise specified. All the main figure experiments were performed in LNCaP cell line, unless otherwise noted.

Compounds and assays

OSMI-2 and OSMI-4 were synthesized in-house (10). AT7519, LDC000067, Palbociclib, RO3306 and PHA848125 were purchased from Selleckchem. Staurosporine was purchased from Abcam. Dinaciclib was from Axon Medchem. NVP2 and SB1317 were obtained from MedChem Express. ATP levels in cells were assessed using the CellTiter-Glo® Luminescent Cell Viability Assay (Promega). Colony-forming assays were performed using the CytoSelect 384-well Cell Transformation Assay (BioCat) according to manufacturer's instructions. Growth rate and cell death activation were evaluated using the Incucyte instrument according to manufacturer's instructions. For detection of cell death activation, we used IncuCyte® Caspase-3/7 Green Reagent for Apoptosis (Essen Biosciences). Cell death activation for **Fig. 2E** and **Suppl. Fig. 3** were performed using the ApoTox-Glo™ Triplex Assay (Promega) according to the manufacturer's instructions (the signal from caspase activity was normalized to signal from viable cells). Cycloheximide (CHX) was used as a positive control to induce cell death. Knockdown experiments were performed using RNAiMax reagent (Sigma). OGT targeting siRNAs were from ThermoFisher Scientific: siOGT_1 s16094 and siOGT_2 s16095 and CDK9 targeting siRNA was from Qiagen (SI00024423).

Protein and mRNA profiling

Samples for western blotting were prepared as previously reported (5). Antibodies used are as follows: from Cell Signaling Technology, Cl-PARP (9541), p-S2/S5-RNA Pol II (4735), p-S2-RNA

Pol II (13499), CDK9 (2316) and OGT (24083). OGA (HPA036141) antibody was obtained from Sigma. Actin (ab49900) and RL2 (ab2739) antibodies were from Abcam.

For RT-qPCR and RNA-seq, RNA isolation was performed using the illustraMiniSpin-kit (GE Healthcare) according to manufacturer's instructions. cDNA was synthesized using the qScript cDNA Synthesis Kit (Quantabio). For spike-in RNA normalization, luciferase mRNA was obtained from Promega (L4561).

High-throughput screen

LNCaP cells were plated into 384-well plate (1000 cells per well). The next day, cells were treated with DMSO or 40 μ M OSMI-2 and compounds from the compound library were separately added to each well. Most of the compounds were screened using a single dose, as pre-defined by the ICCB-Longwood Screening Facility (Boston, Massachusetts). Compounds with well-defined target were often screened in multiple doses, as pre-determined by the ICCB facility. After three days, cells were simultaneously fixed and stained with 4% formaldehyde and Hoechst, respectively. Total fluorescence was recorded with Acumen Laser Scanning Cytometer. The quality of the screen was assessed by calculating the Z'-factor (14) for each plate and was consistently between 0.5 and 1. All treatments were first normalized to DMSO- or OSMI-2- only treatment and are presented as percent of either.

RNA-seq data analysis

Libraries for sequencing were prepared by the Norwegian High Throughput Sequencing Centre using Strand-specific TruSeq RNA-seq library prep kit. Two biological replicates of each condition were used for the analysis. Samples were multiplexed and paired-end sequenced in four lanes with 150bp read length. Sequencing reads were aligned to Hg19 (GRCh37) using STAR (15). Raw counts of reads were mapped to genes using HTSeq counts (<http://htseq.readthedocs.io/en/master/count.html>) and differential expression analysis performed on duplicate samples using DESEQ2 (16). Genes with a p-value of 0.01 were taken forward for Fold Change analysis. RNA-seq BAM files were normalized and converted to BigWig for visualization on IGV 2.0, experimental replicate data tracks were combined and group autoscale used to enable comparable visualization between samples. RNA-seq data has been deposited to the Gene Expression Omnibus (GSE116778).

Comparison of change in mRNA abundance versus mRNA half life

Log2 fold change and Benjamin-Hochberg adjusted p-values obtained from DESeq2 fold change analysis were used to generate volcano plots, and plotted using matplotlib, colored according to half-life based upon data from Schwanhäusser *et al.* (17) mouse homologs. Only genes with homologs and half-life data were included (4212 in total, with 137 genes with mRNA half-life below 4 hours).

Results

Discovery of synthetic lethality between OSMI-2 and a pan-CDK inhibitor AT7519

Both OGT and O-GlcNAc levels are increased in aggressive prostate cancer (5,6), but it is not known if OGT coordinates with specific cellular processes to drive cancer progression. In LNCaP prostate cancer cells, the recently developed OGT inhibitor OSMI-2 (10) dose-dependently decreased total O-GlcNAc and reduced ATP levels by 50% but only modestly affected the proliferation rate (**Fig. 1A-C**). OSMI-2 treatment also resulted in a prominent increase in OGT protein levels, a response previously reported for OGT inhibition (5,10,18). This response represents one of the mechanisms to restore O-GlcNAc homeostasis (18). The reduction in ATP content without a corresponding decrease in cell number implied metabolic adaptations in inhibited cells that sustain proliferation.

To test whether OGT inhibition sensitizes prostate cancer cells to inhibition of other pathways, we screened 5000 biologically active compounds in LNCaP cells with and without cotreatment of OGT inhibitor OSMI-2. The screen was based on cell number as detected via DNA stain. Our strongest hit was AT7519, a pan-CDK inhibitor (**Fig. 1D, 1E** and **Suppl. Fig. 1A**).

We confirmed that OGT inhibition sensitizes LNCaP cells to AT7519 using multiple assays. Live-cell imaging showed that treatment with OSMI-2 and AT7519 blocked the proliferation of LNCaP cells (**Fig. 1F** and **Suppl. Fig. 1B**). Soft agar colony formation assays demonstrated that OSMI-2 combined with AT7519 abolished the ability of LNCaP cells to form colonies (**Fig. 2A, B**). Knockdown of OGT and treatment with AT7519 significantly further decreased ATP levels when compared to any single treatment (**Suppl. Fig. 1C**). We confirmed the anti-proliferative effects of the OGT inhibitor-AT7519 combination in another prostate cancer cell line (PC3), in triple-negative breast cancer cell line (MDAMB231) and in the colon cancer cell line (HCT116, **Suppl. Fig. 2A, B**). These data show that synthetic lethality between OGT inhibition and AT7519 is observed in multiple cancer models.

To better understand the basis for the combined anti-proliferative effects of OSMI-2 and AT7519, we evaluated targets that are affected by AT7519 (19,20). OSMI-2 treatment significantly enhanced

the AT7519-induced decrease in the phosphorylation of protein phosphatase 1 (PP1 α), nucleophosmin 1 (NPM1), and RNA polymerase (Pol) II's carboxy-terminal domain (CTD), which are targets of CDK1, CDK2 and CDK9, respectively (**Fig. 2C**). These effects implied that cell cycle is affected. Combination of AT7519 with OSMI-2 resulted in the accumulation of cells in G2-M phase and decreased the S-phase population by over 50% at 24 hours (**Fig. 2D**). In addition, the sub-G1 population of cells increased for the combination treatment already at 24 hours, and was increased by 5-fold after 48 hours, indicating activation of the cell death response. To confirm cell death activation, we evaluated activation of caspases 3/7 in prostate cancer cells (LNCaP and PC3) and in normal prostate cells (RWPE-1 and PNT2). Strikingly, OSMI-2 potentiated AT7519-induced cell death activation up to 8-fold in prostate cancer cells but the combination did not induce cell death in normal cells (**Fig. 2E and Suppl. Fig. 3**). We further confirmed cell death induction by showing a two fold increase in PARP cleavage in response to OSMI-2-AT7519 combination (**Fig. 2C**).

Taken together, we have identified the CDK inhibitor AT7519 and the OGT inhibitor OSMI-2 as an anti-proliferative combination against cancer cells. Interestingly, OSMI-2 significantly enhanced the effects of AT7519 on its known targets. The observed anti-proliferative effects are explained, at least in part, by activation of the cell death response in cancer cells, while normal prostate cells do not undergo apoptosis under the same treatment. In order to identify the processes that lead to cell death activation, we must focus on events prior to caspase activation.

Inhibition of RNA Pol II CTD kinase CDK9 is lethal in combination with OGT inhibitors

We used transcriptional profiling to probe the basis for synthetic lethality between OGT inhibition and AT7519. Combination treatment with OSMI-2 and AT7519 induced defects in proliferation already at 12 hours after the treatment and cell death was prominent after 24 hours (**Figs. 1F and 2C**). Importantly, OSMI-2 decreased O-GlcNAcylation at 4 hours (**Suppl. Fig. 4A**), thereby providing us with a window of opportunity before decreased proliferation and activation of apoptosis in which we could identify the key events leading to toxicity in cancer cells. As a single agent, short-term treatment with OSMI-2 caused downregulation of pathways related to cell cycle, in agreement with previous reports on OGT inhibitor effects (5,21) (**Suppl. Fig. 4B**). We also noted that OGT inhibition decreases phosphorylation of RNA pol II (**Suppl. Fig. 5**).

OGT expression is regulated through a detained intron-dependent mechanism (18,22) and we assessed if this can be visualized using RNA-seq. Polyadenylated OGT mRNA still contains one intron, intron 4, termed 'detained intron' (22). This intron is rapidly spliced away to enable production of a mature OGT mRNA in a transcription-independent manner (18). As expected,

treatment with OGT inhibitor OSMI-2 led to a depletion of reads mapping to intron 4 (DI4), representing generation of the productive, translation-competent OGT mRNA and predicting upregulation of the OGT protein (**Fig. 3A**). Unexpectedly, AT7519 treatment completely blocked OSMI-2 induced depletion of reads mapping to intron 4, implying defects in OGT regulation in response to OSMI-2 treatment. We confirmed that AT7519 blocks OSMI-2 induced processing of the OGT mRNA and also blunts upregulation of the OGT at the protein level in both LNCaP and PC3 cells (**Fig. 3B, 3C** and **Suppl. Fig. 6**). As expected based on cells' inability to upregulate OGT protein, AT7519 treatment also enhanced the effect of OSMI-2 on total-O-GlcNAc, and we moved on to further explore the RNA-seq data.

Single agent treatment with AT7519 primarily led to downregulation of mRNAs (80% of transcripts) (**Suppl. Fig. 7A**). Combining OSMI-2 with AT7519 increased the number of downregulated genes by almost 400. The top gene ontology (GO) terms under AT7519 treatment were related to gene expression; the same processes were even more enriched in the combination treatment (**Fig. 4A** and **Suppl. Fig. 7B**). Notably, these ontologies are similar to those observed upon CDK9 inhibition in prior studies (23,24). Because AT7519 potently inhibits CDK9 (19), we hypothesized that targeting CDK9 is sufficient to induce synthetic lethality with OGT inhibition.

NVP2 is a CDK9 inhibitor with >700-fold more selectivity for CDK9 than any other kinase (23). Combining either OSMI-2 or OSMI-4, a closely related but more potent OGT inhibitor that became available when we were developing this project (10), with 5-10 nanomolar NVP2 resulted in a complete loss of cellular proliferation, depleted ATP levels and over doubled the activation of cell death response when compared to any single treatment (**Fig. 4B, 4C** and **Suppl. Fig. 8**). On the other hand, OSMI-2 did not potentiate anti-proliferative effects of small molecule inhibitors targeting CDK1, CDK2 or CDK4/6 (**Fig. 4C**). NVP2 is a highly specific CDK9 inhibitor; however, in order to assess whether OGT inhibition sensitizes prostate cancer cells to clinically relevant compounds, we used Dinaciclib and SB1317, two CDK9-inhibitors that have been tested in Phase I-III clinical trials (25). Importantly, OGT inhibition sensitized LNCaP and PC3 prostate cancer cells also to these CDK9 inhibitors (**Fig. 4D** and **Suppl. Fig. 9**). We also used siRNA against CDK9 to confirm the importance of CDK9 for the anti-proliferative effects in combination with OGT inhibition (**Suppl. Fig. 10**). Taken together, targeting CDK9 is sufficient to induce anti-prostate cancer effects in combination with OGT inhibitors.

Targeting OGT potentiates CDK9 inhibitor-induced defects in transcription

We hypothesized that targeting OGT potentiates CDK9 inhibitor effects on cancer cell proliferation due to defects in transcription. OGT glycosylates RNA Pol II CTD on Ser-5 and Ser-7, and OGT

inhibition blocks pre-initiation complex formation in *in vitro* assays (26), while CDK9 phosphorylates RNA Pol II CTD on Ser-2 to promote productive elongation (25). When RNA Pol II activity is inhibited, all mRNA species start to decay, but mRNAs with short half-lives are lost more rapidly (27). If our hypothesis is correct, combining OSMI-2 with a low dose of CDK9 inhibitor should lead to a stronger decline in short half-live mRNAs than targeting CDK9 alone. To test if transcription is decreased globally, we compared previously reported genome-wide mRNA half-life data (17) to our RNA-seq dataset. Based on the data reported by Schwanhaussner *et al.* (2011), we divided all mRNAs into two groups: mRNAs with half-lives less than 4 hours (the time point of RNA collection in our RNA-seq experiment) and those with longer half-lives. AT7519 decreased the abundance of almost all short half-life mRNAs ($p < 0.003$ between AT7519 and OSMI-2; **Fig. 5A**), consistent with the importance of CDK9 in promoting RNA Pol II activity (23,24), and validating our experimental approach. OSMI-2 strongly enhanced the AT7519-induced effect on short half-life mRNAs ($p < 0.0009$ between AT7519-only and AT+OSMI-2; **Fig. 5A** and **Suppl. Fig. 11**).

Genes driven by super-enhancers are hyper-sensitive to decrease in RNA Pol II activity, and the proto-typical example of these genes is MYC, a transcription factor that is deregulated in over half of human cancers (28), and known to be downregulated in response to CDK9 inhibition in prostate cancer cells (29). Combining a low dose of any of the three structurally divergent, clinically relevant CDK9 inhibitors with OGT inhibitor led to an up to 90% decline in the levels of MYC mRNA, and further enhanced the effects of any single treatment by over 50% (**Fig. 5B**). In addition, all of these CDK9 inhibitors blocked OSMI-2 induced splicing and upregulation of the OGT mRNA (**Fig. 5C**). Finally, combining a low dose of any of the three structurally divergent CDK9 inhibitors with OGT inhibitor led to a complete loss of RNA Pol II CTD Ser-2 phosphorylation, the site modified by CDK9 (**Fig. 5D**). To conclude, small molecule inhibition of OGT augments CDK9 inhibitor effects on transcription, which explains the anti-cancer effects of this combination (**Fig. 5E**). However, at the same time, this raises concerns of on-target negative effects on normal cells.

Combined inhibition of OGT and CDK9 is lethal to prostate cancer organoids

We used organoid tissue culture system to evaluate if combined inhibition of OGT and CDK9 has potential as anti-cancer therapy. Organoid tissue culture recapitulates structural and functional aspects of the *in vivo* counterpart (30), and prostate cancer organoids retain both epigenomic and transcriptomic concordance with their corresponding tumors in patients (13). These features make organoids an excellent tool for validation of candidate therapies. Castration-resistant prostate cancer (CRPC) is a major challenge in clinical setting and we used three CRPC spheroid models to show

that OGT inhibition potentiates the anti-proliferative effects of CDK9 inhibition in these cells (**Fig. 6A and Suppl. Figs. 12 and 13**). In addition, combination of OGT and CDK9 inhibitors led to an almost complete loss of proliferation of prostate cancer organoids derived from a metastatic prostate cancer patient (**Fig. 6B**). Importantly, combined inhibition of OGT and CDK9 was not toxic to normal prostate cells that grow in similar rate as LNCaP-95 and C4-2 spheroids in the 3D tissue culture system (**Fig. 6C**). We also noted that OGT inhibition shows strong anti-proliferative effects on prostate cancer cells as a single agent. These data validate the results generated in the conventional tissue culture system, and confirm that combined inhibition of OGT and CDK9 has anti-proliferative effects specifically on prostate cancer but not on normal prostate cells.

Discussion

Our entry point to this project was sensitization screen that led to the discovery of synthetic lethal interaction between compounds targeting OGT and CDK9. Based on our data and existing literature, we propose that the observed synthetic lethality between inhibitors of OGT and CDK9 is specific to cancer cells that are dependent on high levels of transcription (**Fig. 5E**). Inhibition of OGT blocks RNA pol II entry into the promoters (31), and targeting O-GlcNAcase inhibits transcription elongation in nuclear extract system (32). Remarkably, OGA inhibitors are progressing to clinical trials (33), and it may be possible to induce similar synthetic lethality between inhibitors targeting OGA and CDK9, as we report here for simultaneous inhibition of OGT and CDK9. Our model also proposes that inhibitors targeting either CDK7 or CDK12, the two other major CTD kinases, should also be lethal in combination with OGT inhibitors.

OGT inhibition enhances the effects induced by targeting CDK9. High dose OGT inhibition decreases phosphorylation of RNA pol II on the CDK9-targeted Ser-2 (**Suppl. Fig. 5**), and by combining low dose OGT and CDK9 inhibitors, we see a 5-fold decrease in the Ser-2 phosphorylated form of RNA Pol II (**Figs. 2C and 5D**). We show that targeting OGT enhances the effects induced by CDK9 inhibitors on highly transcribed genes such as c-MYC, but single agent inhibition of OGT has only modest effects on transcription (**Figs. 5B**). Previously we showed that OGT also post-translationally controls the levels of c-MYC (5,34), and OGT can thereby control the levels of key drivers of proliferation by affecting both transcription and protein stability.

The mechanistic underpinnings of the role of OGT in regulating RNA Pol II activity have not been comprehensively described. OGT may prime CTD phosphorylation during transcription initiation or provide hindrance for unscheduled phosphorylation, as phosphorylation and glycosylation are mutually exclusive on the same residue, and O-GlcNAc removal is an ATP-dependent step during transcription initiation (31,35). To formally test this, one would have to trap

the RNA Pol II complexes at the gene promoters / gene body in a synchronized manner, and detect the presence of glycosylation and phosphorylation in a site- and a location-specific manner, an experiment that goes beyond the scope of this manuscript: discovery of the synthetic lethal interaction of combined inhibition of OGT and other cellular processes. To conclude, OGT and CDK9 act in consecutive steps during transcription initiation, and simultaneous inhibition of both leads to a further decrease in transcription, which we propose as the anti-cancer mechanism of action for this combination (**Fig. 5E**).

In characterizing the observed synthetic lethal interaction, we noted that inhibition of CDK9 activity blocks splicing of the OGT detained intron (DI, **Fig. 3A, 3B and 5C**). This is the first time that CDK9 is linked to regulation of DIs, and raises the possibility that global dysregulation of DI-containing genes is a hallmark of cancers exhibiting altered activity of CDK9.

CDK9 inhibitors are being evaluated as cancer therapy and our work showed that OGT inhibition can potentiate anti-proliferative effects of this promising class of therapeutics while sparing noncancerous cells. Specific OGT inhibitors used in this study induce anti-proliferative effects selectively on prostate cancer organoids, and we propose that OGT inhibitors can be used to prime cancer cells to other targeted therapies.

Acknowledgements

Authors are grateful to members of the Walker laboratory and Dr Brian Lewis (NIH) for the critical feedback on the manuscript. We also thank the ICCB-Longwood Screening Facility for the assistance in the screen. We are grateful for the support that was received to complete this work as follows: HMI for the Norwegian Cancer Society travel Fellowships (ID 159970 – 2014 and ID 181596 – 2016), SESM for the National Institutes of Health (F32 GM117704), AU for the Norwegian Cancer Society (198016-2018), ML's work is supported by NIH grants (R01CA131945, R01CA187918, DoD PC160357, DoD PC180582, P50CA211024), and the Prostate Cancer Foundation, CJT receives support from the intramural programs of the Center for Cancer Research, National Cancer Institute and the Division of Preclinical Innovation, National Center for Advancing Translational Sciences of that National Institutes of Health, IGM is a member of the Prostate Cancer UK/Movember Centre of Excellence (CEO13_2-004 supported RES) and also supported by the John Black Charitable Foundation and the Norwegian Research Council (230559) and Norwegian Cancer Society (Project nr. 4521627) and SW for the National Institutes of Health R01 GM094263.

References

1. Yang X, Qian K. Protein O-GlcNAcylation: emerging mechanisms and functions. *Nature reviews Molecular cell biology* **2017**;18(7):452-65 doi 10.1038/nrm.2017.22.
2. Hart GW. Nutrient regulation of signaling and transcription. *The Journal of biological chemistry* **2019**;294(7):2211-31 doi 10.1074/jbc.AW119.003226.
3. Hanover JA, Krause MW, Love DC. Bittersweet memories: linking metabolism to epigenetics through O-GlcNAcylation. *Nat Rev Mol Cell Biol* **2012**;13(5):312-21 doi 10.1038/nrm3334.
4. Siegel RL, Miller KD, Jemal A. Cancer statistics, 2018. *CA: a cancer journal for clinicians* **2018**;68(1):7-30 doi 10.3322/caac.21442.
5. Itkonen HM, Minner S, Guldvik IJ, Sandmann MJ, Tsourlakis MC, Berge V, *et al.* O-GlcNAc transferase integrates metabolic pathways to regulate the stability of c-MYC in human prostate cancer cells. *Cancer research* **2013**;73(16):5277-87 doi 10.1158/0008-5472.CAN-13-0549.
6. Kamigaito T, Okaneya T, Kawakubo M, Shimojo H, Nishizawa O, Nakayama J. Overexpression of O-GlcNAc by prostate cancer cells is significantly associated with poor prognosis of patients. *Prostate cancer and prostatic diseases* **2014**;17(1):18-22 doi 10.1038/pcan.2013.56.
7. Kazemi Z, Chang H, Haserodt S, McKen C, Zachara NE. O-linked beta-N-acetylglucosamine (O-GlcNAc) regulates stress-induced heat shock protein expression in a GSK-3beta-dependent manner. *The Journal of biological chemistry* **2010**;285(50):39096-107 doi 10.1074/jbc.M110.131102.
8. O'Donnell N, Zachara NE, Hart GW, Marth JD. Ogt-dependent X-chromosome-linked protein glycosylation is a requisite modification in somatic cell function and embryo viability. *Molecular and cellular biology* **2004**;24(4):1680-90.
9. Shafi R, Lyer SPN, Ellies LG, O'Donnell N, Marek KW, Chui D, *et al.* The O-GlcNAc transferase gene resides on the X chromosome and is essential for embryonic stem cell viability and mouse ontogeny. *P Natl Acad Sci USA* **2000**;97(11):5735-9 doi DOI 10.1073/pnas.100471497.
10. Martin SES, Tan ZW, Itkonen HM, Dubeau DY, Paulo JA, Janetzko J, *et al.* Structure-Based Evolution of Low Nanomolar O-GlcNAc Transferase Inhibitors. *Journal of the American Chemical Society* **2018** doi 10.1021/jacs.8b07328.
11. Itkonen HM, Urbanucci A, Martin SE, Khan A, Mathelier A, Thiede B, *et al.* High OGT activity is essential for MYC-driven proliferation of prostate cancer cells. *Theranostics* **2019**;9(8):2183-97 doi 10.7150/thno.30834.
12. Gao D, Vela I, Sboner A, Iaquina PJ, Karthaus WR, Gopalan A, *et al.* Organoid cultures derived from patients with advanced prostate cancer. *Cell* **2014**;159(1):176-87 doi 10.1016/j.cell.2014.08.016.
13. Puca L, Bareja R, Prandi D, Shaw R, Benelli M, Karthaus WR, *et al.* Patient derived organoids to model rare prostate cancer phenotypes. *Nat Commun* **2018**;9(1):2404 doi 10.1038/s41467-018-04495-z.
14. Zhang JH, Chung TD, Oldenburg KR. A Simple Statistical Parameter for Use in Evaluation and Validation of High Throughput Screening Assays. *Journal of biomolecular screening* **1999**;4(2):67-73 doi 10.1177/108705719900400206.
15. Dobin A, Davis CA, Schlesinger F, Drenkow J, Zaleski C, Jha S, *et al.* STAR: ultrafast universal RNA-seq aligner. *Bioinformatics* **2013**;29(1):15-21 doi 10.1093/bioinformatics/bts635.
16. Love MI, Huber W, Anders S. Moderated estimation of fold change and dispersion for RNA-seq data with DESeq2. *Genome biology* **2014**;15(12):550 doi 10.1186/s13059-014-0550-8.
17. Schwanhauss B, Busse D, Li N, Dittmar G, Schuchhardt J, Wolf J, *et al.* Global quantification of mammalian gene expression control. *Nature* **2011**;473(7347):337-42 doi 10.1038/nature10098.
18. Park SK, Zhou X, Pendleton KE, Hunter OV, Kohler JJ, O'Donnell KA, *et al.* A Conserved Splicing Silencer Dynamically Regulates O-GlcNAc Transferase Intron Retention and O-GlcNAc Homeostasis. *Cell reports* **2017**;20(5):1088-99 doi 10.1016/j.celrep.2017.07.017.
19. Squires MS, Feltell RE, Wallis NG, Lewis EJ, Smith DM, Cross DM, *et al.* Biological characterization of AT7519, a small-molecule inhibitor of cyclin-dependent kinases, in human tumor cell lines. *Molecular cancer therapeutics* **2009**;8(2):324-32 doi 10.1158/1535-7163.MCT-08-0890.

20. Santo L, Vallet S, Hideshima T, Cirstea D, Ikeda H, Pozzi S, *et al.* AT7519, A novel small molecule multi-cyclin-dependent kinase inhibitor, induces apoptosis in multiple myeloma via GSK-3 β activation and RNA polymerase II inhibition. *Oncogene* **2010**;29(16):2325-36 doi 10.1038/onc.2009.510.
21. Barkovskaya A, Seip K, Hilmarsdottir B, Maelandsmo GM, Moestue SA, Itkonen HM. O-GlcNAc Transferase Inhibition Differentially Affects Breast Cancer Subtypes. *Sci Rep* **2019**;9(1):5670 doi 10.1038/s41598-019-42153-6.
22. Boutz PL, Bhutkar A, Sharp PA. Detained introns are a novel, widespread class of post-transcriptionally spliced introns. *Genes & development* **2015**;29(1):63-80 doi 10.1101/gad.247361.114.
23. Olson CM, Jiang B, Erb MA, Liang Y, Doctor ZM, Zhang Z, *et al.* Pharmacological perturbation of CDK9 using selective CDK9 inhibition or degradation. *Nature chemical biology* **2018**;14(2):163-70 doi 10.1038/nchembio.2538.
24. Muhar M, Ebert A, Neumann T, Umkehrer C, Jude J, Wieshofer C, *et al.* SLAM-seq defines direct gene-regulatory functions of the BRD4-MYC axis. *Science* **2018**;360(6390):800-5 doi 10.1126/science.aao2793.
25. Sonawane YA, Taylor MA, Napoleon JV, Rana S, Contreras JI, Natarajan A. Cyclin Dependent Kinase 9 Inhibitors for Cancer Therapy. *J Med Chem* **2016**;59(19):8667-84 doi 10.1021/acs.jmedchem.6b00150.
26. Ranuncolo SM, Ghosh S, Hanover JA, Hart GW, Lewis BA. Evidence of the involvement of O-GlcNAc-modified human RNA polymerase II CTD in transcription in vitro and in vivo. *The Journal of biological chemistry* **2012**;287(28):23549-61 doi 10.1074/jbc.M111.330910.
27. Yang E, van Nimwegen E, Zavolan M, Rajewsky N, Schroeder M, Magnasco M, *et al.* Decay rates of human mRNAs: correlation with functional characteristics and sequence attributes. *Genome research* **2003**;13(8):1863-72 doi 10.1101/gr.1272403.
28. Boffo S, Damato A, Alfano L, Giordano A. CDK9 inhibitors in acute myeloid leukemia. *Journal of experimental & clinical cancer research : CR* **2018**;37(1):36 doi 10.1186/s13046-018-0704-8.
29. Itkonen HM, Poulouse N, Walker S, Mills IG. CDK9 Inhibition Induces a Metabolic Switch that Renders Prostate Cancer Cells Dependent on Fatty Acid Oxidation. *Neoplasia* **2019**;21(7):713-20 doi 10.1016/j.neo.2019.05.001.
30. Tuveson D, Clevers H. Cancer modeling meets human organoid technology. *Science* **2019**;364(6444):952-5 doi 10.1126/science.aaw6985.
31. Lewis BA, Burlingame AL, Myers SA. Human RNA Polymerase II Promoter Recruitment in Vitro Is Regulated by O-Linked N-Acetylglucosaminyltransferase (OGT). *The Journal of biological chemistry* **2016**;291(27):14056-61 doi 10.1074/jbc.M115.684365.
32. Resto M, Kim BH, Fernandez AG, Abraham BJ, Zhao K, Lewis BA. O-GlcNAcase Is an RNA Polymerase II Elongation Factor Coupled to Pausing Factors SPT5 and TIF1 β . *The Journal of biological chemistry* **2016**;291(43):22703-13 doi 10.1074/jbc.M116.751420.
33. Selnick HG, Hess JF, Tang C, Liu K, Schachter JB, Ballard JE, *et al.* Discovery of MK-8719, a Potent O-GlcNAcase Inhibitor as a Potential Treatment for Tauopathies. *J Med Chem* **2019**;62(22):10062-97 doi 10.1021/acs.jmedchem.9b01090.
34. Itkonen HM, Gorad SS, Duveau DY, Martin SE, Barkovskaya A, Bathen TF, *et al.* Inhibition of O-GlcNAc transferase activity reprograms prostate cancer cell metabolism. *Oncotarget* **2016**;7(11):12464-76 doi 10.18632/oncotarget.7039.
35. Kelly WG, Dahmus ME, Hart GW. RNA polymerase II is a glycoprotein. Modification of the COOH-terminal domain by O-GlcNAc. *The Journal of biological chemistry* **1993**;268(14):10416-24.
36. Vassilev LT, Tovar C, Chen S, Knezevic D, Zhao X, Sun H, *et al.* Selective small-molecule inhibitor reveals critical mitotic functions of human CDK1. *Proceedings of the National Academy of Sciences of the United States of America* **2006**;103(28):10660-5 doi 10.1073/pnas.0600447103.
37. Brasca MG, Amboldi N, Ballinari D, Cameron A, Casale E, Cervi G, *et al.* Identification of N,1,4,4-tetramethyl-8-[[4-(4-methylpiperazin-1-yl)phenyl]amino]-4,5-dihydro-1H-pyrazolo[4,3-

- h]quinazoline-3-carboxamide (PHA-848125), a potent, orally available cyclin dependent kinase inhibitor. *Journal of medicinal chemistry* **2009**;52(16):5152-63 doi 10.1021/jm9006559.
38. Fry DW, Harvey PJ, Keller PR, Elliott WL, Meade M, Trachet E, *et al.* Specific inhibition of cyclin-dependent kinase 4/6 by PD 0332991 and associated antitumor activity in human tumor xenografts. *Molecular cancer therapeutics* **2004**;3(11):1427-38.

Figure legends

Figure 1. Small molecule inhibitor screen to identify compounds that sensitize cells to OGT inhibitor OSMI-2. **A)** Cells were treated for 24 hours and analyzed using western blotting. Densitometry was used to determine the intensity of the bands. **B)** Cells were treated as indicated and ATP levels were assessed using the CellTiter-Glo assay. Data shown is an average of three biological replicates with SEM and t-test was used to assess statistical significance (* $p < 0.05$, ** $p < 0.01$). **C)** Growth rate of cells was recorded using live-cell imaging. Data shown is an average of three biological replicates with SEM and t-test was used to assess statistical significance (* $p < 0.05$). **D)** Small molecule inhibitor screen. Cells were treated with either DMSO or OSMI-2, and an additional compound. After 3 days, the relative cell number was measured based on Hoechst nuclear stain. Data is presented as %-of DMSO- or OSMI-2-only treated cells (AT7519 highlighted in red). **E)** Structure of AT7519, EC₅₀-values from (19). **F)** Growth rate of LNCaP cells was recorded using live-cell imaging (average of three biological replicates with SEM; Student's t-test was used to assess the statistical significance between combination against any other treatment, * $p < 0.05$, ** $p < 0.01$). Note that the data for DMSO and OSMI-2 treatments are the same in main figure 1C and 1F.

Figure 2. OGT inhibition enhances the effects of pan-CDK inhibitor AT7519. **A)** Representative images of LNCaP cells grown in soft-agar for 7 days and treated as indicated. **B)** Relative cell number based on soft-agar colony forming assay (average of 4 biological replicates with SEM; Student's t-test was used to assess statistical significance, * $p < 0.05$, ** $p < 0.01$, *** $p < 0.001$). **C)** Cells were treated for 24 hours and samples were analyzed using western blot. Densitometry was used to determine signal intensity (average of 3 biological replicates with SEM, statistical analysis as in B). **D)** Propidium iodide staining and flow cytometry were used to determine cell cycle distribution after the indicated treatments. The data shown is an average of three biological replicates with SEM. OSMI-2: 40 μ M; AT7519: 0.5 μ M. G1 Phase makes up the rest of the percentage up to 100% and is omitted for clarity in this figure. **E)** Cell death activation after 48 hours of treatment was assessed using ApoTox-Glo™ Triplex Assay. The signal from caspase activity was normalized to signal from viable cells (average of three biological replicates with SEM; cycloheximide (CHX) served as a positive control to induce cell death).

Figure 3. Pan-CDK inhibitor AT7519 blocks splicing of the OGT mRNA. **A)** Integrative Genomics Viewer was used to visualize RNA-seq data for OGT locus from cells treated as indicated. OGT detained intron 4 is highlighted. **B)** Schematic of RT-qPCR assay for detection of the OGT mRNA containing detained intron 4 (left) and productive isoform (right); small arrows denote primers used. Cells were treated as indicated and analyzed using RT-qPCR. **C)** Cells were treated as indicated and analyzed using western blot. Densitometry was used to determine signal intensity (average of 3 biological replicates with SEM; Student's t-test was used to assess statistical significance, * $p < 0.05$, *** $p < 0.001$).

Figure 4. CDK9 inhibitors are synthetically lethal with OGT inhibition. **A)** Gene ontology enrichment using the STRING database for the top most downregulated genes based on RNA-seq, as indicated in Suppl. Fig. 7. **B)** OSMI-4 sensitizes cells to highly specific CDK9 inhibitor NVP2 (23). Growth rate of cells was recorded using live-cell imaging (average of three biological replicates with SEM; Student's t-test was used to assess the statistical significance). **C)** Cells were treated as indicated for three days and cell viability was assessed using CellTiter-Glo reagent. RO3306 is an inhibitor of CDK1 (36), PHA848125 is an inhibitor of CDK2 (37), Palbociclib is a dual inhibitor of CDK4 and CDK6 (38), while NVP2 is a specific inhibitor of CDK9 (23). Student's t-test was used to evaluate the statistical significance (** $p < 0.01$, *** $p < 0.001$). **D)** Growth rate of

cells was recorded using live-cell imaging. Data shown is an average of three biological replicates with SEM. Student's t-test was used to evaluate statistical significance. Note that DMSO and OSMI-4 treatments are from the same experiments in both left and right.

Figure 5. Targeting OGT augments CDK9 inhibition induced effects on transcription in prostate cancer cells. **A)** Comparison of fold change of all mRNAs with half-lives less than 4 hours as reported in (17) after treatment with OSMI-2, AT7519 or OSMI-2+AT7519. Statistical comparison represents result of two-sample t-test of ratios for all genes meeting half-life cut-offs (n=127 genes). **B)** OSMI-2 (40μM) augments the effects of three structurally unrelated CDK9 inhibitors (20nM NVP2, 20nM Dinaciclib and 100nM SB1317) on MYC mRNA levels and **C)** OGT mRNA splicing (average of 3 biological replicates with SEM; Student's t-test was used to evaluate the statistical significance (*p<0.05, *p<0.01 and ***p<0.001). **D)** OSMI-4 (20μM) enhances the effects of CDK9 inhibitors on RNA-Pol II Ser-2 phosphorylation. Cells were treated for 24 hours and analyzed using western blot (represents 2 biological replicates). **E)** Model of RNA Pol II CTD modifications along the gene body. The main point of activity for OGT and RNA Pol II CTD kinase CDK9 are highlighted along with some of the inhibitors used in this study.

Figure 6. OGT inhibition augments CDK9 inhibitor effects on organoids derived from metastatic prostate cancer patients. **A-C)** OGT inhibitor OSMI-2, or the more potent OGT inhibitor OSMI-4, that came available during preparation of this manuscript, augments the effects of CDK9 inhibitors NVP2 and Dinaciclib on proliferation of prostate cancer organoids. Organoids were allowed to form and imaged prior to start of the treatment, and imaged again at the end of the treatment; the graphs present fold change in size and Student's t-test was used to evaluate the significance of the data, *p<0.05, **p<0.01 and ***p<0.001. The percentage value in the low left corner reports the area that was covered by organoids. The length of the scale bar is 0.09mm. Representative images for LNCaP-95, C4-2 and 22RV1 spheroids are provided in Suppl. Fig. 13.

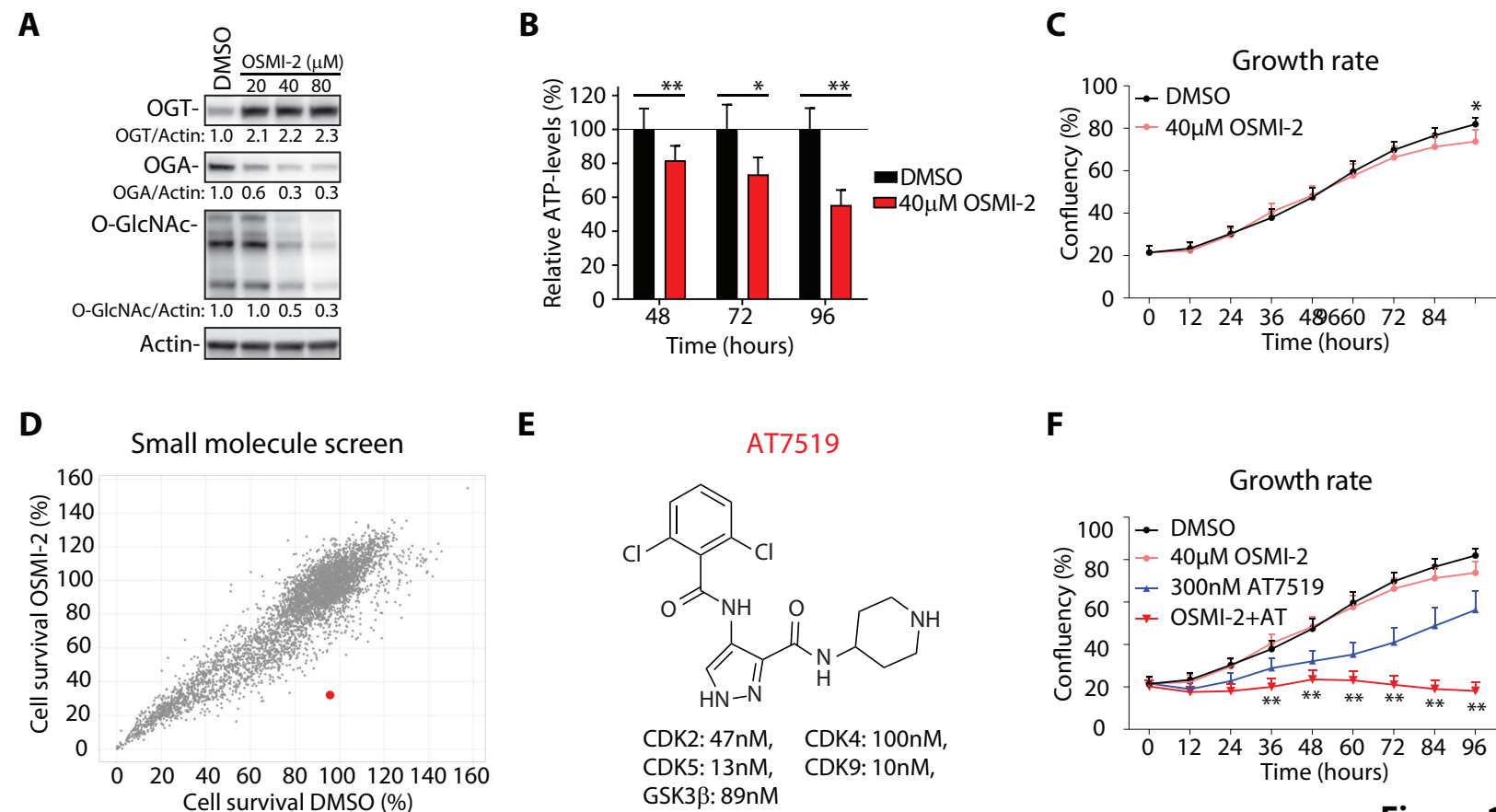
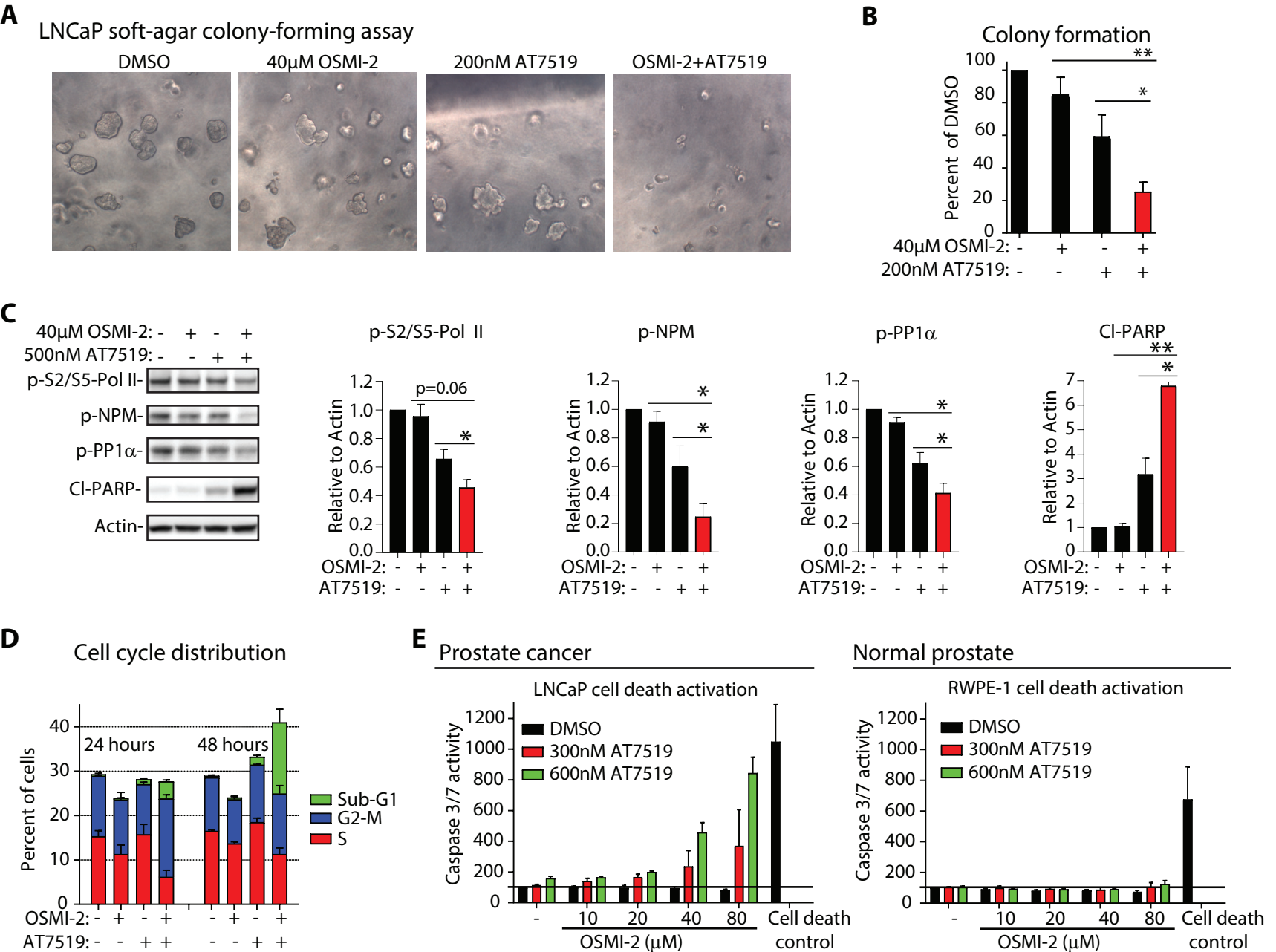
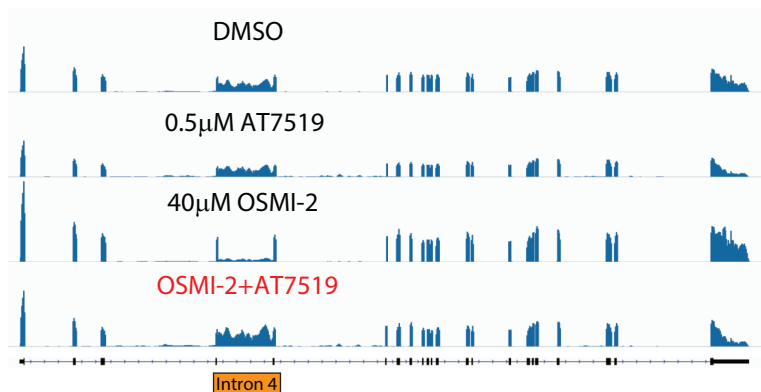


Figure 1



A

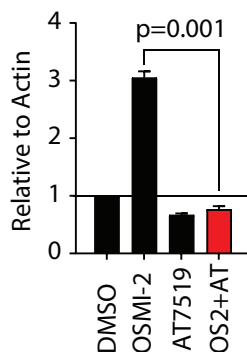
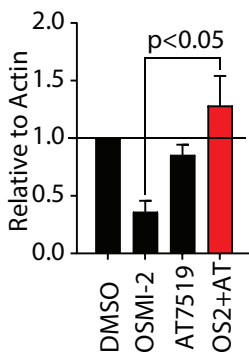
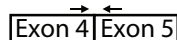
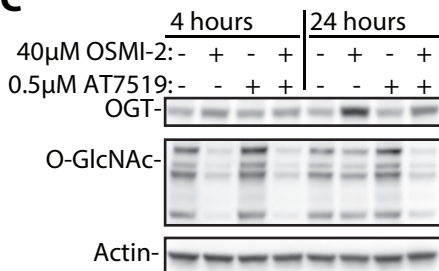
RNA-seq 4 hours treatment

**B**

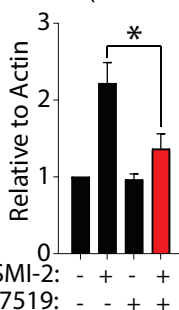
OGT detained intron



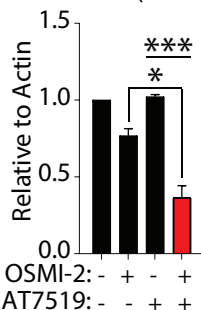
OGT productive isoform

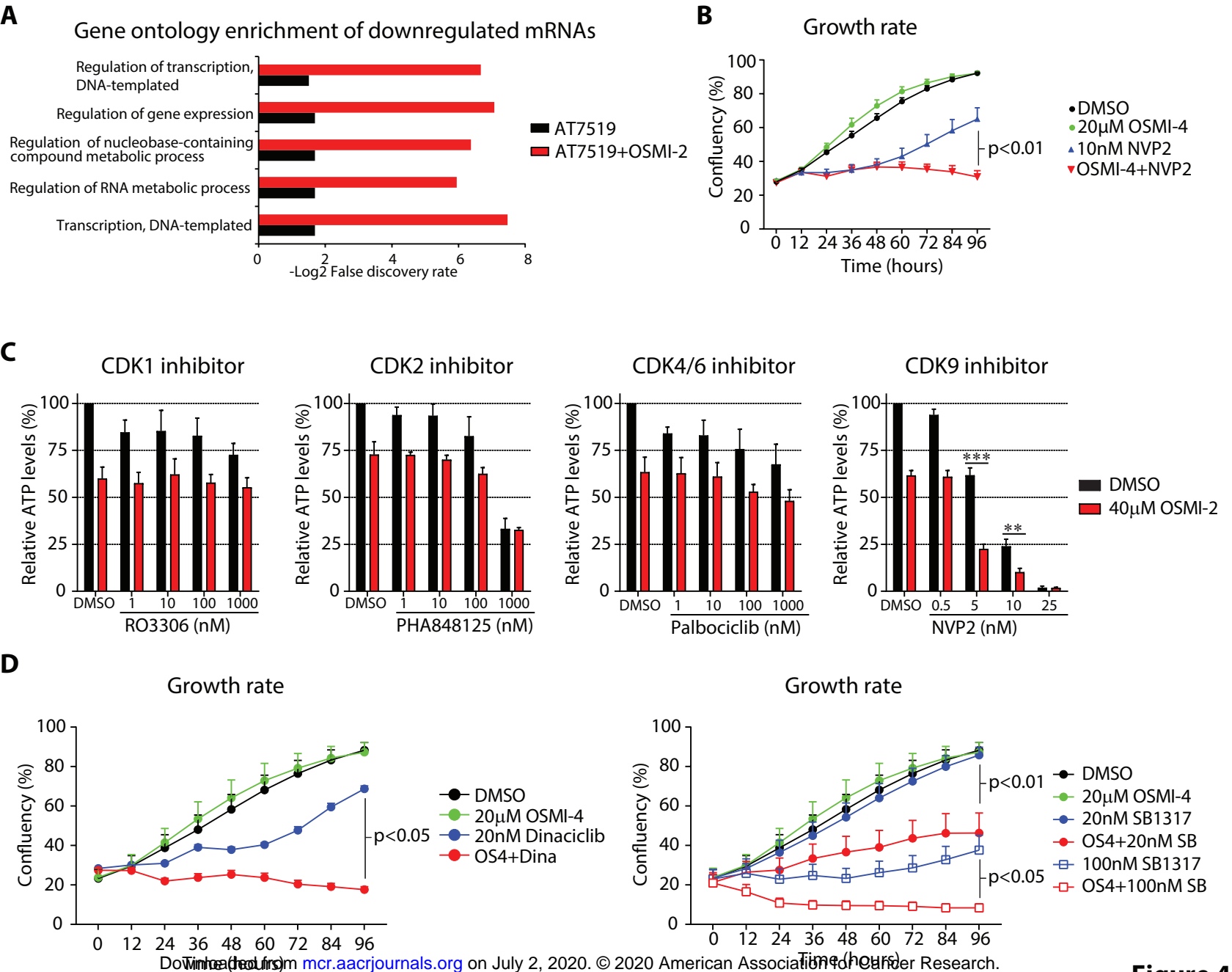
**C**

OGT (24 hours)



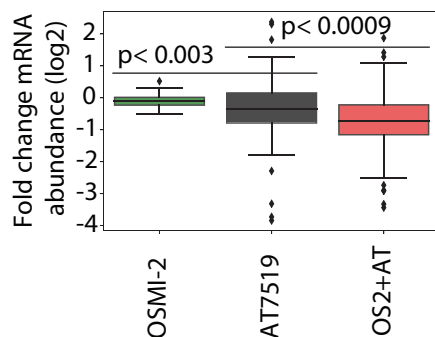
O-GlcNAc (24 hours)



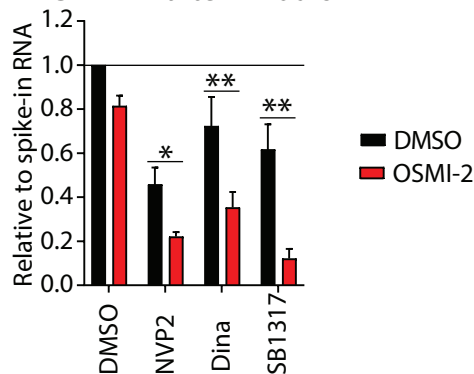


A

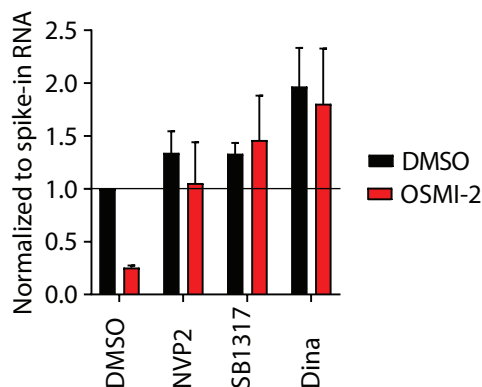
mRNAs with half-life <4 hours

**B**

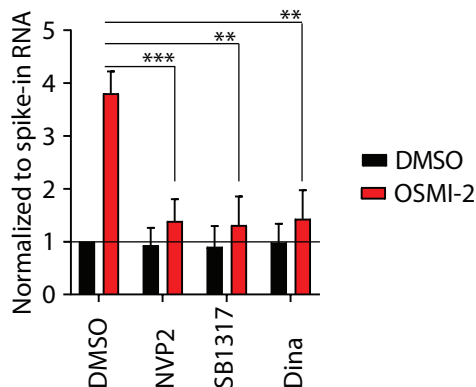
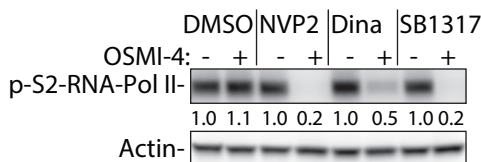
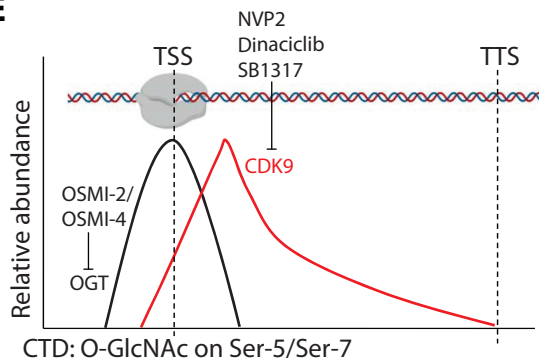
MYC mRNA after 4 hours

**C**

OGT detained intron



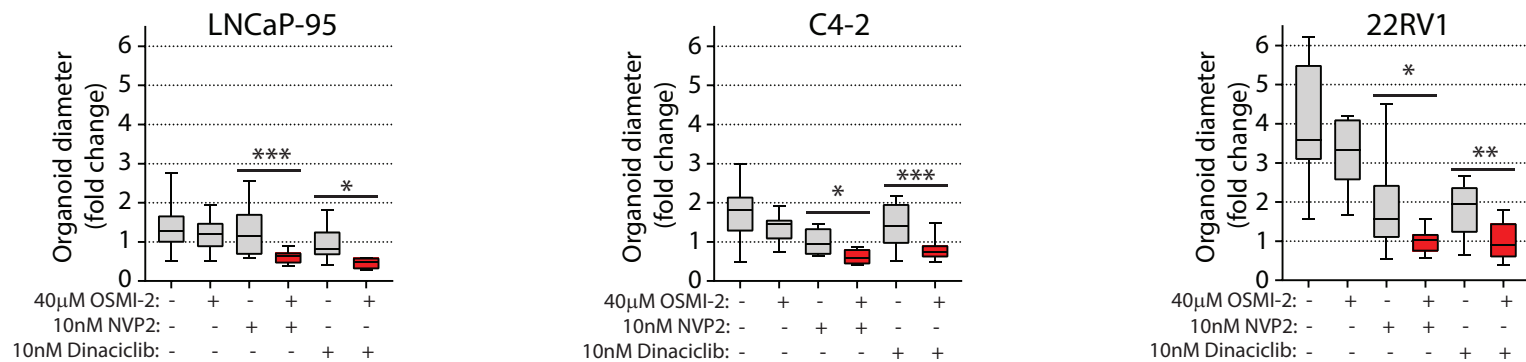
OGT productive isoform

**D****E**

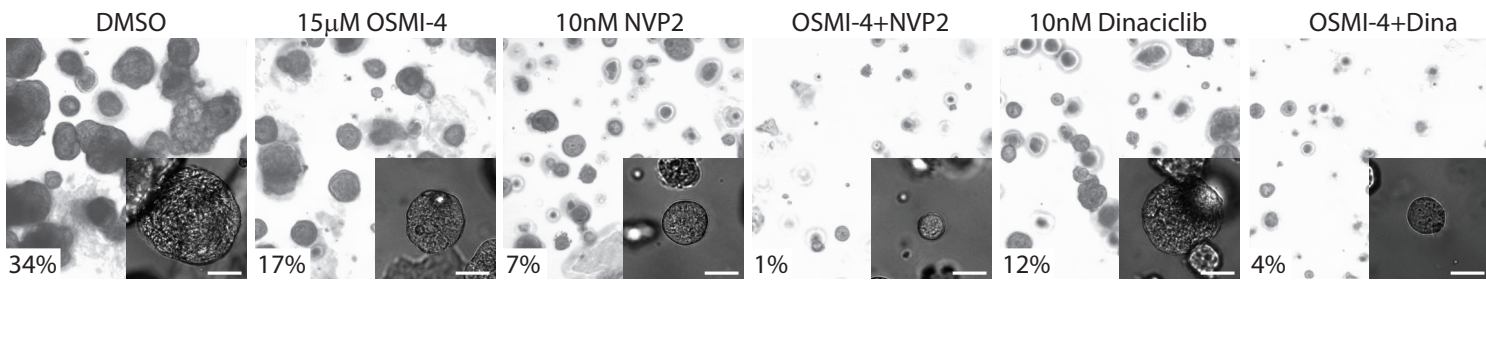
CTD: O-GlcNAc on Ser-5/Ser-7

CTD: Phosphorylation on Ser-2

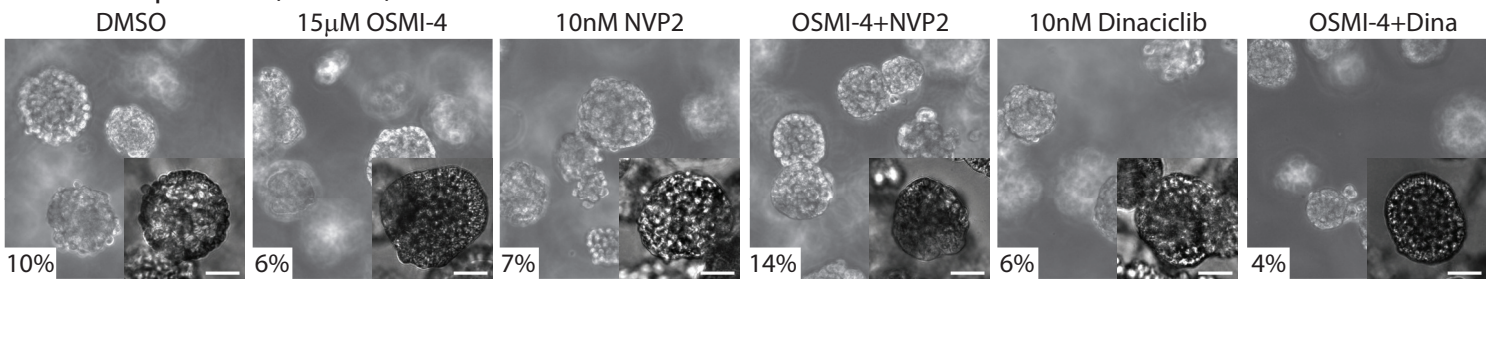
A Models of castration-resistant prostate cancer



B Metastatic prostate cancer (MSK-PCA3)



C Normal prostate (RWPE-1)



Molecular Cancer Research

Inhibition of O-GlcNAc transferase renders prostate cancer cells dependent on CDK9

Harri M Itkonen, Ninu Poulouse, Rebecca E Steele, et al.

Mol Cancer Res Published OnlineFirst July 1, 2020.

Updated version	Access the most recent version of this article at: doi: 10.1158/1541-7786.MCR-20-0339
Supplementary Material	Access the most recent supplemental material at: http://mcr.aacrjournals.org/content/suppl/2020/07/01/1541-7786.MCR-20-0339.DC1
Author Manuscript	Author manuscripts have been peer reviewed and accepted for publication but have not yet been edited.

E-mail alerts	Sign up to receive free email-alerts related to this article or journal.
Reprints and Subscriptions	To order reprints of this article or to subscribe to the journal, contact the AACR Publications Department at pubs@aacr.org .
Permissions	To request permission to re-use all or part of this article, use this link http://mcr.aacrjournals.org/content/early/2020/07/01/1541-7786.MCR-20-0339 . Click on "Request Permissions" which will take you to the Copyright Clearance Center's (CCC) Rightslink site.